

Optical Properties of Lead-Free $\text{Cs}_2\text{AgInCl}_6$: Bi/SiO₂ Nanocrystals with Double Perovskite Crystal Structure

© M.D. Miruschenko¹, I.A. Timkina¹, V.R. Nautran¹, I.V. Margarian¹, E.A. Grigoryev², S.A. Cherevko¹, E.V. Ushakova¹

¹ ITMO University,
197101 St. Petersburg, Russia

² St. Petersburg State University,
199034 St. Petersburg, Russia

e-mail: m@miruschenko.ru

Received May 30, 2022

Revised June 03, 2022

Accepted June 03, 2022

The optical characteristics of lead-free nanocrystals with a crystal structure of the double perovskite type with the chemical composition $\text{Cs}_2\text{AgInCl}_6$, doped with bismuth and coated with silicon dioxide were studied, and the possibility of their further application was shown. The optical properties of the nanocrystals under study are analyzed by absorption and luminescence spectroscopy, including those with time resolution. Images were obtained using a scanning electron microscope. The influence of the amount of silicon dioxide precursor addition on the optical properties and morphology of lead-free nanocrystals was established. It is shown that the observed broad photoluminescence band is associated with the occurrence of self-trapped excitons in such nanocrystals. To demonstrate the possibility of practical application of these nanocrystals a light-emitting device based on them was developed and constructed. The light emitting device has a wide emission spectrum close to warm white light.

Keywords: LEDs, lead-free perovskites, double perovskites, nanocrystals, photoluminescence.

DOI: 10.21883/EOS.2022.08.54776.3748-22

Introduction

To date, one of the attractive active materials are structures with a crystal lattice of the perovskite type. Initially, perovskites were considered for use in photonics as part of transistors and light-emitting diodes [1]. Later, perovskites were used in dye-sensitized solar cells as a replacement for molecular dye, and it was also found that they can be used with great success for charge transfer [2].

More common are the so-called nanocrystals (NC) with a crystal structure of the perovskite type (PNC). This is due to the limitations occurring in bulk perovskites and films: in the former a large number of defects occur during growth, which leads to the almost complete absence of radiative relaxation channels, and, in the latter, the probability of nonradiative transitions significantly increases at grain boundaries, which also leads to the deterioration of radiative properties [3]. It is regarded that it is possible to fine tune the size and shape of PNCs, which makes it possible to obtain cubic NCs, nanoplates, nanosheets, and nanowires. A big advantage of PNC is the possibility of changing the composition, structure, and size not only during synthesis, but also through post-synthesis processing, for example, through ion exchange or shell growth.

Despite a large number of positive properties, most PNCs contain lead, and also have not very high stability in a humid air atmosphere, which leads to the limitation of their possible areas of application. Therefore, the creation of new lead-free NC compositions and their stabilization for

storage and use under ambient conditions are becoming increasingly important tasks. Lead-containing PNCs can be replaced by lead-free NCs with a crystal structure of the double perovskite type (lfPNC), in which lead is replaced by two more safe cations. One of such compositions is $\text{Cs}_2\text{AgInCl}_6$, the quantum yield of which can reach 50% [4] at a certain doping. For stabilization under ambient conditions, the method of growing a silicon oxide shell on the surface of lfPNC can be used [5]. The improvement of the optical properties of lfPNC and their preservation under conditions of long-term operation is possible due to the optimization of syntheses, selection of compositions, and surface passivation, which currently makes them one of the materials most relevant for research.

In this paper we study the optical properties of $\text{Cs}_2\text{AgInCl}_6$ lfPNC doped with bismuth and coated with silicon dioxide. The influence on these properties and on the morphology of lfPNC was determined by the volume of addition of tetraethylorthosilicate used to grow the silicon dioxide shell. The fundamental possibility of practical use of the NCs under study in a polystyrene matrix as a light-emitting layer in a down-conversion-LED is shown.

Experimental part

Synthesis of NC $\text{Cs}_2\text{AgInCl}_6$: Bi/SiO₂

During the lfPNC synthesis with the composition $\text{Cs}_2\text{AgInCl}_6$, doped with 1% Bi and covered with a silicon

dioxide shell (abbreviated name $\text{Cs}_2\text{AgInCl}_6:\text{Bi}/\text{SiO}_2$), such precursors as Cs_2CO_3 (99.9%, Sigma Aldrich, Darmstadt, Germany), 1-octadecene ($\text{CH}_2=\text{CH}(\text{CH}_2)_{15}\text{CH}_3$, 1-octadecene, ODE, 90%, Sigma Aldrich, Darmstadt, Germany), oleic acid ($\text{C}_{17}\text{H}_{33}\text{COOH}$, oleic acid, OA, 85–92%, Fisher Scientific, Loughborough, UK), AgNO_3 (99.9%, Sigma Aldrich, Darmstadt, Germany), InCl_3 (99.99%, Sigma-Aldrich, Darmstadt, Germany), BiCl_3 (99.99%, Sigma Aldrich, Darmstadt, Germany), oleylamine ($\text{CH}_3(\text{CH}_2)_7\text{CH}=\text{CH}(\text{CH}_2)_7\text{CH}_2\text{NH}_2$, oleylamine, OLA, 80–90%, Sigma Aldrich, Darmstadt, Germany), HCl (analytical pure, VEKTON, St.-Petersburg, Russia), tetraethyl orthosilicate ($(\text{C}_2\text{H}_5\text{O})_4\text{Si}$, TEOS, 99.99%, Sigma Aldrich, Darmstadt, Germany) were used. Prior to synthesis the precursors were not subjected to additional purification. Hexane (C_6H_{14} , 99.5%, EKOS 1, Moscow, Russia) was also used during the work.

Most often, for the synthesis of PNC and lFPNC the classical method of hot injection is used [6]. BsPNC $\text{Cs}_2\text{AgInCl}_6:\text{Bi}/\text{SiO}_2$ studied in this paper were obtained by a simplified method, in which no preliminary synthesis of cesium oleate occurred. To obtain them, the following precursors are loaded into the flask, mixed and heated to 95°C for 1 h in vacuum: 162.8 mg Cs_2CO_3 , 61 mg AgNO_3 , 80 mg InCl_3 , 1.1 mg BiCl_3 , 14 mL ODE, 2 mL OA and 1 mL OLA. Further cooling to room temperature, addition of 0.5 mL HCl and further heating to 195°C were performed. This is followed by slow cooling to room temperature, and at 60°C TEOS is added in a volume of 0 to 500 μL . Further in paper the designation SX is used, where X is the volume of the TEOS additive in μL . The TEOS addition makes it possible to grow the silicon dioxide shell on the lFPNC surface [5], which prevents anion exchange of various halogens between individual lFPNCs. Growing the silicon dioxide shell makes it possible to obtain structures of the core–shell type.

To separate the synthesized lFPNCs from the unreacted precursors the centrifugation was performed for 20 min at 6000 rot/min. After that, lFPNCs were washed several times with acetone and redissolved in hexane.

Introduction of NC $\text{Cs}_2\text{AgInCl}_6:\text{Bi}/\text{SiO}_2$ into a polystyrene matrix

Toluene (C_7H_8 , 99.5%, EKOS-1, Moscow, Russia) and polystyrene ($[\text{CH}_2\text{CH}(\text{C}_6\text{H}_5)]_n$, Sigma-Aldrich, Darmstadt, Germany) were used when lFPNC $\text{Cs}_2\text{AgInCl}_6:\text{Bi}/\text{SiO}_2$ was introduced into the polystyrene matrix. The bsPNA incorporation begins with the dissolution of 60 mg of polystyrene in 1 mL of toluene at a temperature of 60°C , after which 850 μL of bsPNA supernatant is added to the resulting solution. Next, layer-by-layer application of 100 μL of the resulting solution onto a quartz substrate takes place. Each subsequent layer was applied after the previous layer drying. Drying is also carried out at a temperature of 60°C for faster evaporation of the toluene.

Research methods

The optical properties of the samples were studied on the UV-3600 spectrophotometer (Shimadzu, Japan), Cary Eclipse (Varian, USA) and FP 8200 (Jasco, Japan) spectrofluorimeters, and the MicroTime 100 laser scanning microscope (LSM) (PicoQuant, Germany) equipped for studying solutions with a 3-power lens ($NA = 0.1$) and a pulsed diode laser with a wavelength of 405 nm. The PL decay curves were approximated by the sum of the exponents:

$$I(t) = \sum_i A_i \exp\left(-\frac{t}{\tau_i}\right), \quad (1)$$

where A_i are amplitudes, and τ_i are decay times of the components. Average decay times were calculated using the formula

$$\tau_{av} = \frac{\sum_i A_i \tau_i^2}{\sum_i A_i \tau_i}. \quad (2)$$

To obtain information about the band gap (BG) width, the method of spectrum linearization near the absorption edge was used using the Tauc formulas [7]. The morphology of the obtained samples was estimated from images obtained with the AURIGA scanning electron microscope (Zeiss, Germany), working distance is 4.1 mm, accelerating voltage is 10 kV, resolution is 1.74 nm. The size of individual lFPNCs was determined by the Gwyddion software package using the watershed algorithm [8]. In this paper, the following values were used: size — root of the area of the observed surface of NCs, mode — maximum in distributions by size, average — arithmetic mean of sizes from all lFPNCs, maximum — size of the largest lFPNCs.

The homogeneity of the resulting light-emitting device was assessed using images obtained on a confocal LSM-710 (Zeiss, Germany).

Results and discussion

To obtain information about the effect of the volume of the TEOS additive (due to which the silicon dioxide shell grows) on the properties of the samples, their optical characteristics and morphology were studied.

The optical characteristics of the studied lFPNCs were evaluated from their absorption and PL spectra, as well as from the PL decay times. For optical measurements the samples were dispersed in hexane.

The absorption and PL spectra are shown in Fig. 1, *a, b, c*.

All samples have two peaks in the absorption spectrum near 330 and 370 nm, and at wavelengths above 400 nm the absorption rapidly decreases. In the literature absorption features similar to those obtained are explained by exciton absorption [9] or direct *s*–*p*-transition in Bi [10]. In this case, a large Stokes shift could indicate an indirect transition, but at Bi content of less than 25% the transition should be direct [11,12]. In this case the PL bands turned

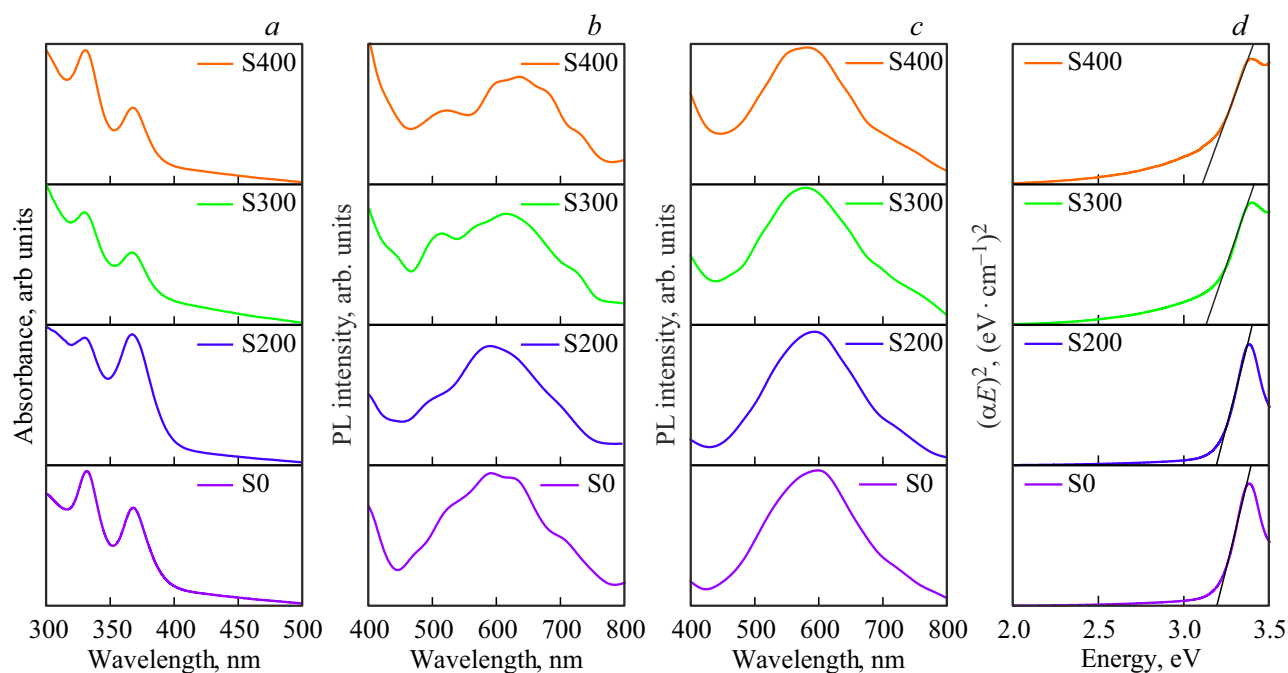


Figure 1. Absorption (a) and PL spectra of samples upon excitation at wavelengths corresponding to the second (about 330 nm) (b) and first (about 370 nm) (c) long-wavelength peaks in the absorption spectra. The Tauc plots (d).

Table 1. Optical characteristics of studied samples

Sample	Volume TEOS, mL	Position of absorption peaks, nm	Position of PL peaks / their half-width (excitation), nm	PL decay time, ns	Width BG, eV
S400	0.4	328, 366	617 / 161 (330) 576 / 142 (367)	3.6	3.1
S300	0.3	328, 365	610 / 146 (330) 581 / 147 (367)	3.7	3.13
S200	0.2	324, 367	592 / 165 (330) 589 / 157 (367)	5.4	3.19
S0	0	331, 367	596 / 159 (330) 589 / 159 (367)	6.1	3.19

out to be even wider than for samples obtained by the classical method of hot injection [5]. Such broadband and near-white emission usually comes from self-trapped excitons (STE) [13]. Unlike PL from free excitons or charge carriers (free states), luminescence from STE is usually broad and has a significant Stokes shift relative to the long-wavelength maximum in the absorption spectrum. The distortion of the STE- state with respect to the ground state, determined by the distance between them, broadens the emission spectrum. Also, the stabilization of STE- states with respect to the free state (self-trapping depth) contributes to the Stokes shift [14]. In this case, transitions from states of free charge carriers to states of free excitons occur in about 600 fs, and from states of free excitons to STE-states — in 400 fs [13]. STE- states

themselves, which provide such a wide PL band, can be formed due to the Jahn-Teller distortion lattice cells. In the case of $\text{Cs}_2\text{AgInCl}_6$, such a distortion occurs on AgCl_6 octahedron [15].

Based on the fact that the lFPNCs obtained in this paper were synthesized by a simplified method, it can be concluded that in the course of such synthesis additional distortion of lattice cells occurred, leading to even greater stabilization of STE- states compared to lFPNCs obtained by hot injection.

To determine the BG width diagrams of $\alpha E^{1/n}$ versus the absorbed photon energy (E) were plotted (Fig. 1, d). The PL decay curves were approximated by a biexponential function (1). The average PL decay times were calculated

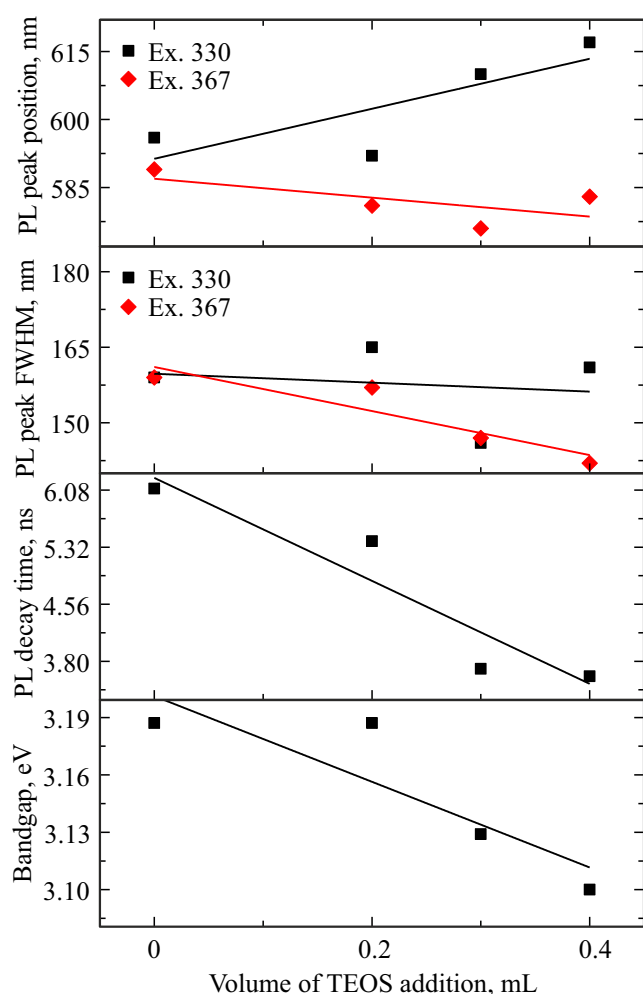


Figure 2. Main parameters of PL and BG vs. volume of TEOS addition upon excitation at 330 and 367 nm.

using formula (2). Generalized data for all samples are given in Table 1.

Fig. 2 shows the dependencies plotted according to the data of Table 1.

From the data in Table 1 and Fig. 2 for the PL decay times and the BG width one can distinguish decreasing dependences, close to linear, on the volume of the TEOS addition. The positions of the maxima and the full width at half maximum (FWHM) of the PL bands are almost independent of the TEOS additions.

Note that this synthesis leads to reproducible optical characteristics of lfpNC. The properties stability was investigated for the sample without TEOS (S0). It turned out that the positions of the absorption peaks and PL peaks remain unchanged for more than 6 months when the sample is stored in a refrigerator ($t = 5^{\circ}\text{C}$).

On SEM-images it was expected to see structures consisting of near-cubic particles with sizes of about 12–13 nm, similar to those obtained in the paper [5]. Fig. 3 shows the original SEM- image of sample S400, which shows both

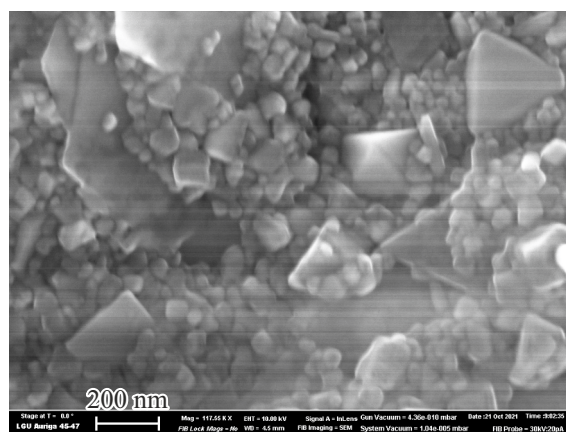


Figure 3. Example of SEM-image before processing.

Table 2. Statistical data from SEM- images of samples

Sample	Volume of TEOS, ml	Mode, nm	Mean, nm	Maximum, nm
S400	0.4	61	71	333
S300	0.3	23	38	350
S0	0	18	23	68

NCs with expected sizes and structures with large sizes and different shapes.

In the process of images processing the horizontal bands and noise present in the images were removed, after which the particles were separated using a watershed algorithm and masking. To characterize the samples from their SEM- images using the Gwyddion software [8], PNC size distributions were obtained based on the generated masks (Fig. 4).

Table 2 shows the statistical data obtained from the distributions for these samples.

Based on the data in Table 2 the statistical parameters vs. the volume of the TEOS additive were plotted (Fig. 5) with the indication of the confidence interval obtained from the histogram data (Fig. 4). For the studied samples the linear relationship is observed between the volume of TEOS additive and morphology. Sample S0 does not have large scattering in sizes as the other two samples.

From Fig. 5, we can conclude that the size of lfpNC is linearly related to the volume of TEOS additive.

It is quite difficult to create a light emitting device, the emission of which covers the entire visible range, based on a single light emitting material. BspNCs are well suited for such devices because they have a wide luminescence band, as shown in Fig. 1. To create the light-emitting device (down-conversion-LED) based on the studied lfpNCs, we used a commercial ultraviolet (UV) LED with an emission wavelength of 367 nm, corresponding to the first long-wavelength maximum in the absorption spectrum of the studied lfpNCs, and work voltage from 3.2 to

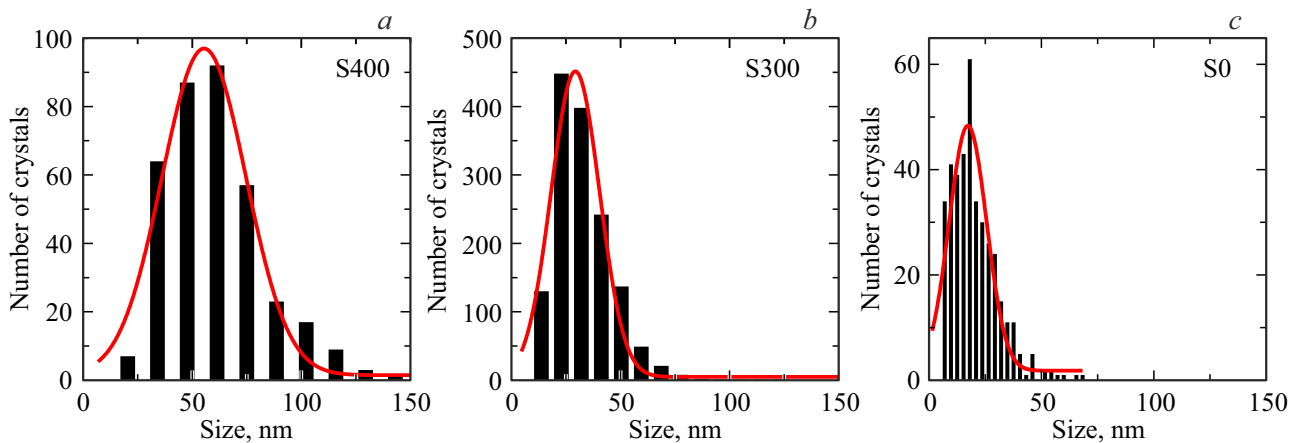


Figure 4. NC size distributions for samples S400 (a), S300 (b) and S0 (c).

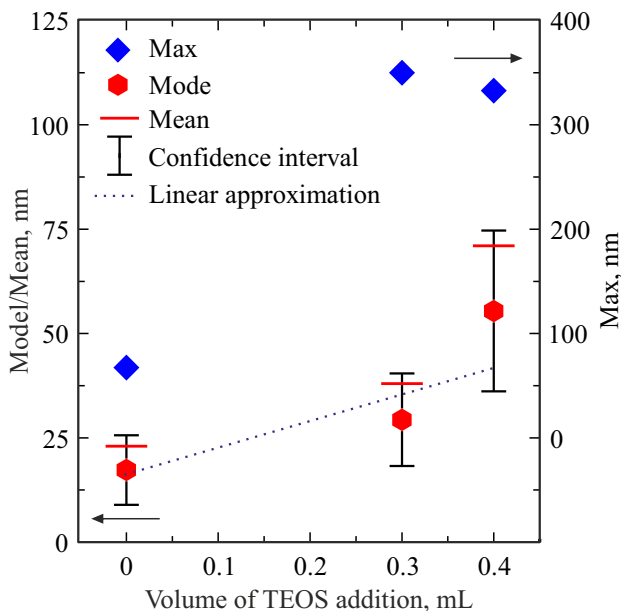


Figure 5. Statistical parameters of samples S400, S300 and S0 vs. volume of TEOS additive.

3.7 V. The emission spectrum of this commercial LED is shown in Fig. 6, a, and Fig. 6, b shows the scheme of down-conversion-LED obtained in the paper.

An opaque limiter is installed around the diffuser of the commercial LED, on top of the limiter a 10×10 mm quartz plate is installed, which is used as a substrate for further application of the light-emitting layer with lfpnc. The light-emitting layer consists of polystyrene, in which lfpncs S400 are embedded. In such light-emitting device due to the absorption of UV emission from a commercial LED by layer of lfpnc in a polystyrene matrix, the PL of the lfpncs themselves is excited. Fig. 7, a shows an image of light-emitting layer consisting of lfpnc in polystyrene matrix obtained using LSM. In this case, the PL of lfpnc and the UV light from the commercial LED passing through

the light-emitting layer contribute to the total emission of down-conversion-LED, the spectrum of which is shown in Fig. 7, b. Further, based on the spectrum and using method from [16] the points were plotted on the CIE 1931 chromatic diagram (7, c).

From Fig. 7, a one can understand that, on the whole, the distribution of lfpncs in the bulk of the polystyrene matrix is rather uniform. From the inset in Fig. 7, b it can be seen that the emission of the resulting down-conversion-LED is close to warm white emission, which is confirmed by the chromatic diagram, from which one can estimate the glow temperature as 3,500 K.

Conclusion

In the present paper we synthesized lfpncs having the chemical composition $\text{Cs}_2\text{AgInCl}_6$, doped with bismuth and coated with a silicon dioxide shell by a simplified (relative to the classical) hot injection method. It was found that the mixing of precursors and their further heating in one flask lead to the formation of nanocrystals, the properties of which do not depend on the size and its dispersion. The observed broad PL band is associated with the NCs formation with internal deformations and stresses, which leads to the occurrence of self-trapped excitons in NCs. It was established that the volume of additives has practically no effect on the properties and morphology of the samples. The lfpncs synthesized in this paper in the polystyrene matrix were used as an active light-emitting layer in down-conversion-LED based on commercial UV chip. The obtained light-emitting device has a wide emission spectrum, close to warm white light with a color temperature of about 3,500 K.

Funding

The study was funded by a grant from NIRMA Physical and Technical Mega-Faculty of ITMO University. SEM-measurements were carried out on the equipment of

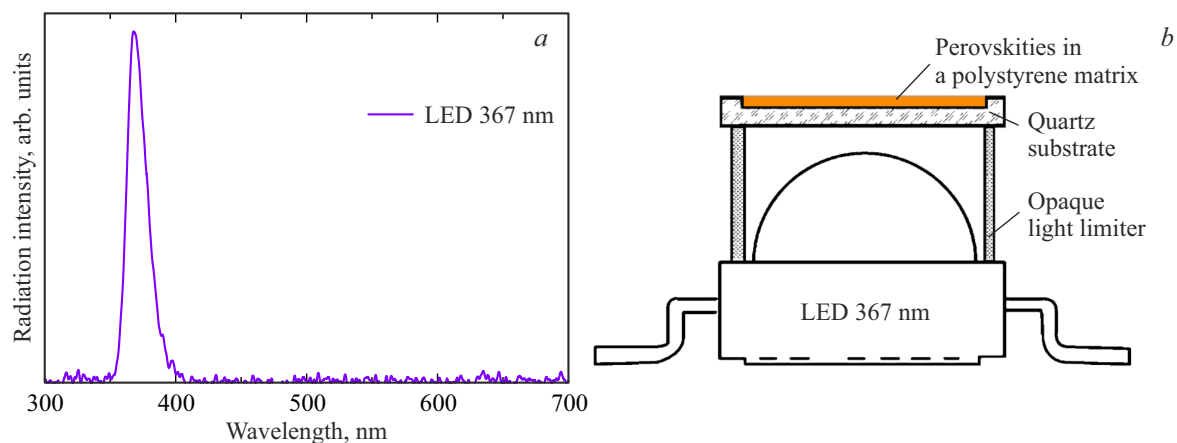


Figure 6. The emission spectrum of the used LED (a). Scheme of light-emitting device (down-conversion-LED) based on commercial LED (b).

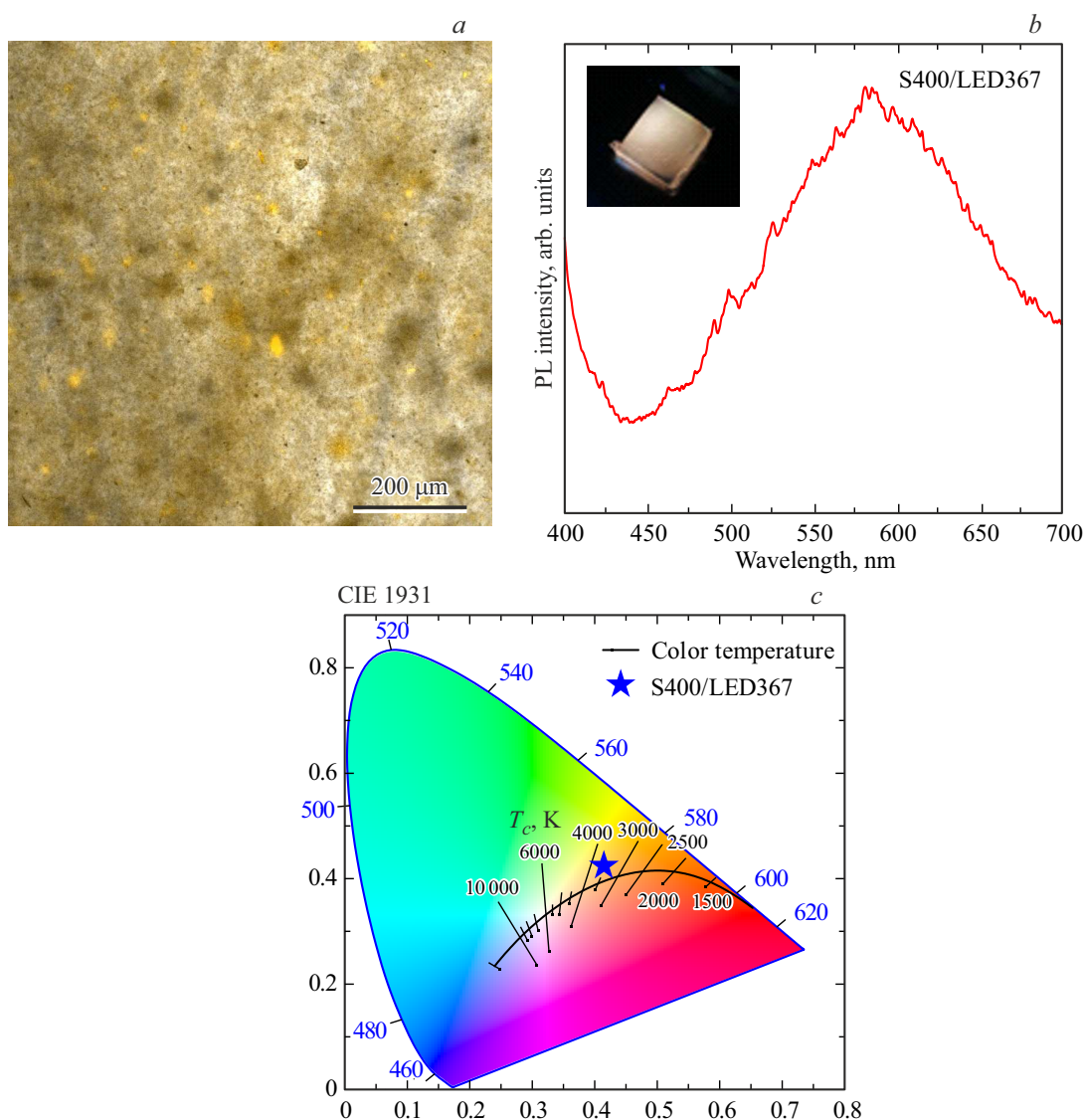


Figure 7. LSM-image combined from the signals in the luminescent channel and the transmission channel, lfpNC in a polystyrene matrix (a). The emission spectrum of the created light-emitting device (b). Appearance of the received device during its operation (b, inset). CIE 1931 chromatic diagram showing the position of the created down-conversion-LED (c).

the Interdisciplinary Resource Center in the direction of Nanotechnology of St. Petersburg State University Science Park.

Conflict of interest

The authors declare that they have no conflict of interest.

References

- [1] D.B. Mitzi, S. Wang, C.A. Feild, C.A. Chess, A.M. Guloy. *Science*, **267** (5203), 1473 (1995). DOI: 10.1126/SCIENCE.267.5203.1473
- [2] A. Kojima, K. Teshima, Y. Shirai, T. Miyasaka. *J. Am. Chem. Soc.*, **131** (17), 6050 (2009). DOI: 10.1021/JA809598R
- [3] D.W. de Quilletes, S.M. Vorpahl, S.D. Stranks, H. Nagaoka, G.E. Eperon, M.E. Ziffer, H.J. Snaith, D.S. Ginger. *Science*, **348** (6235), 683 (2015). DOI: 10.1126/SCIENCE.AAA5333
- [4] W. Zheng, R. Sun, Y. Liu, X. Wang, N. Liu, Y. Ji, L. Wang, H. Liu, Y. Zhang. *ACS Appl. Mater. Interfaces*, **13** (5), 6404 (2021). DOI: 10.1021/ACSAMI.0C20230
- [5] S.A. Cherevko, R.R. Azizov, A.V. Sokolova, V.R. Nauran, M.M. Miruschenko, I.A. Arefina, M.A. Baranov, D.A. Kurdyukov, E.Y. Stovpiaga, V.G. Golubev, A.V. Baranov, E.V. Ushakova. *Nanomaterials*, **11** (1), 119 (2021). DOI: 10.3390/NANO11010119
- [6] Y. Liu, Y. Jing, J. Zhao, Q. Liu, Z. Xia. *Chem. Mater.*, **31** (9), 3333 (2019). DOI: 10.1021/ACS.CHEMMATER.9b00410
- [7] Tauc. *J. Mater. Res. Bull.*, **3** (1), 37 (1968). DOI: 10.1016/0025-5408(68)90023-8
- [8] P. Klapetek, D. Nečas, C. Anderson. *Gwyddion user guide* [Electronic source]. URL: <http://gwyddion.net/download/user-guide/gwyddion-user-guide-en.pdf>
- [9] R.S. Lamba, P. Basera, S. Bhattacharya, S. Sapra. *J. Phys. Chem. Lett.*, **10** (17), 5173 (2019). DOI: 10.1021/ACS.JPCLETT.9b02168
- [10] Y. Bekenstein, J.C. Dahl, J. Huang, W.T. Osowiecki, J.K. Swabeck, E.M. Chan, P. Yang, A.P. Alivisatos. *Nano Lett.*, **18** (6), 3502 (2018). DOI: 10.1021/ACS.NANOLETT.8B00560
- [11] B. Yang, X. Mao, F. Hong, W. Meng, Y. Tang, X. Xia, S. Yang, W. Deng, K. Han. *J. Am. Chem. Soc.*, **140** (49), 17001 (2018). DOI: 10.1021/JACS.8B07424
- [12] D. Manna, T.K. Das, A. Yella. *Chem. Mater.*, **31** (24), 10063 (2019). DOI: 10.1021/ACS.CHEMMATER.9B02973
- [13] M.D. Smith, H.I. Karunadasa. *Acc. Chem. Res.*, **51** (3), 619 (2018). DOI: 10.1021/ACS.ACCOUNTS.7B00433
- [14] T. Hu, M.D. Smith, E.R. Dohner, M.-J. Sher, X. Wu, M.T. Trinh, A. Fisher, J. Corbett, X.-Y. Zhu, H.I. Karunadasa, A.M. Lindenberg. *J. Phys. Chem. Lett.*, **7** (12), 2258 (2016). DOI: 10.1021/ACS.JPCLETT.6B00793
- [15] J. Luo, X. Wang, S. Li, J. Liu, Y. Guo, G. Niu, L. Yao, Y. Fu, L. Gao, Q. Dong, C. Zhao, M. Leng, F. Ma, W. Liang, L. Wang, S. Jin, J. Han, L. Zhang, J. Etheridge, J. Wang, Y. Yan, E.H. Sargent, J. Tang. *Nature*, **563** (7732), 541 (2018). DOI: 10.1038/S41586-018-0691-0
- [16] J. Cohen, G. Wysecki, W.S. Stiles. *Am. J. Psychol.*, **81** (1), 128 (1968). DOI: 10.2307/1420820